Micromagnetic description of the spin spiral in Fe double-layer stripes on W(110)

S. Meckler,[1,*] O. Pietzsch,[1] N. Mikuszeit,[2] and R. Wiesendanger[1]

[1]*Institute of Applied Physics and Microstructure Advanced Research Center Hamburg, University of Hamburg, Jungiusstrasse 11, DE-20355 Hamburg, Germany*

[2]*Instituto Madrileño de Estudios Avanzados en Nanociencia, IMDEA-Nanociencia, Campus Universidad Autónoma de Madrid, ES-28049 Madrid, Spain*

(Received 13 October 2011; revised manuscript received 22 December 2011; published 31 January 2012)

The surface spin spiral in the Fe double layer on W(110) is investigated within the framework of micromagnetic theory. It is shown that the previously suggested restriction to homogeneous spiral profiles and the consideration of the demagnetizing energy within the concept of an effective magnetic anisotropy do not allow for a consistent description of all experimental observations. After a detailed discussion of the model approaches in the literature, an extended micromagnetic model is proposed. The respective model parameters are derived as fit parameters to experimental data. It is shown that the presented model overcomes the deficiencies of all previous approaches. In particular, it reproduces the hitherto unexplained divergence of the spiral period in narrow Fe double-layer stripes of a width below 15 nm.

DOI: 10.1103/PhysRevB.85.024420 PACS number(s): 75.70.Ak, 75.60.Ch, 75.25.−j, 68.37.Ef

I. INTRODUCTION

During the past decade, the surface spin spiral in the Fe double layer (DL) on W(110) was the subject of numerous experimental and theoretical studies.[1–13] One major focus of these investigations was put on the identification of the magnetic interactions that drive the formation of the spiral state. Within the framework of micromagnetic theory, the magnetic exchange stiffness A, the effective anisotropy parameter K_{eff}, and the Dzyaloshinskii-Moriya[14–17] (DM) vector D were determined. However, it turned out that, depending on the underlying model approach, the values of these parameters vary tremendously, with none of the suggested models being powerful enough to reproduce all experimental observations in a consistent way. Consequently, quantitative conclusions concerning the parameter values and thus the driving forces of the spiral ground state remained puzzling.

In particular, we are aware of four approaches that have been discussed in the context of the theoretical description of the Fe DL on W(110).[1–4] Table I compares these approaches with respect to their power to reproduce the measured right-rotating cycloidal character of the spin spiral,[3] the spiral period,[8,10] the domain-wall width,[10] the domain-wall direction,[2] the magnetic field dependence,[1] the temperature dependence of the spiral state,[8,9] the stripe-width dependence of the spiral period, and vanishing of the spiral state for stripe widths below about 15 nm.[8,10] Agreement (disagreement) of the theoretical results in Refs. 1–4 with the experimental observations is indicated by + (−) signs. The table indicates that all models give predictions being contradictory to at least some of the experimental observations. In particular, none of the models can explain the measured temperature and stripe-width dependence of the spin spiral state. These major deficiencies certainly call for a theoretical description, which goes beyond the previously suggested models and is powerful enough to reproduce all measured properties in a consistent way.

Except for the case of Ref. 2, the models cited in Table I rely on the calculation of the total energy density per magnetic volume on the basis of a micromagnetic continuum model:

$$\varepsilon\left[\phi\left(x\right)\right] = \frac{\int_0^{\lambda} A\dot{\phi}^2 + D\dot{\phi} + K_{\mathrm{c}}\cos^2\phi \; dx}{\lambda} + \varepsilon_{\mathrm{d}}\left[\phi\left(x\right)\right]. \quad (1)$$

Here, $\phi(x)$ describes the spiral profile, i.e., the angle of the magnetization with respect to the propagation direction, as a function of the position x along the spiral. The parameter λ indicates the period length. The three summands of the integrand describe the energy density contributions of magnetic exchange, the DM interaction, and the crystalline anisotropy. The functional $\varepsilon_{\mathrm{d}}\left[\phi\left(x\right)\right]$ refers to the energy density of the demagnetizing field.

In contrast to Refs. 1,3, and 4, the Monte Carlo simulations in Ref. 2 rely on a set of discrete spins and are not based on a micromagnetic continuum theory. Nevertheless, the results can be translated into the micromagnetic parameters of a corresponding continuum model based on Eq. (1). This allows for a direct comparison to the results of Refs. 1,3, and 4 as summarized in Table I.

The demagnetizing energy density ε_{d} in Eq. (1) can be split into two parts:

$$\varepsilon_{\mathrm{d}} = \underbrace{\frac{\int_V \frac{\mu_0}{2} {M_{\mathrm{z}}}^2 \, dV}{V}}_{\varepsilon_{\mathrm{d}}^0} - \underbrace{\frac{\int_V \frac{\mu_0}{2} \mathbf{H}_{\mathrm{d}}^* \cdot \mathbf{M} \, dV}{V}}_{\varepsilon_{\mathrm{d}}^*}. \quad (2)$$

This splitting relies on the idea that the demagnetizing field $\mathbf{H}_{\mathrm{d}}$ can be written as a superposition of two field contributions, i.e., $\mathbf{H}_{\mathrm{d}} = \mathbf{H}_{\mathrm{d}}^0 + \mathbf{H}_{\mathrm{d}}^*$. In particular, $\mathbf{H}_{\mathrm{d}}^0$ can be chosen such that $\mathbf{H}_{\mathrm{d}}^0 = -\mathbf{M}_{\mathrm{z}}$, with $\mathbf{M}_{\mathrm{z}}$ being the projection of the magnetization onto the direction of the surface normal. V refers to the magnetic volume of the sample. For the special case $\varepsilon_{\mathrm{d}}^* = 0$ (homogeneous magnetization), Eq. (1) reduces to

$$\varepsilon\left[\phi\left(x\right)\right] = \frac{\int_0^{\lambda} A\dot{\phi}^2 + D\dot{\phi} + K_{\mathrm{eff}}\cos^2\phi \; dx}{\lambda}. \quad (3)$$

Here, $K_{\mathrm{eff}} = K_{\mathrm{c}} - \frac{\mu_0}{2} M_{\mathrm{S}}^2$ is an effective anisotropy parameter that considers the effect of both the crystalline anisotropy and the energy density contribution of $\varepsilon_{\mathrm{d}}^0$. In particular, the approximation does not account for $\varepsilon_{\mathrm{d}}^*$ and the possibility of

TABLE I. Agreement (+) and disagreement (−) of current models with experimental observations.

	Ref. 1	Ref. 2	Ref. 3	Ref. 4
Cycloidal character	−	−	+	+
Rotational sense	−	−	+	+
Spiral period	−	+	+	−
Domain-wall width	+	+	+	−
Domain-wall direction	−	+	+	+
Magnetic field dependence	+	−	−	−
Vanishing spin contrast at elevated temperature	−	−	−	−
Stripe-width dependence of the spiral period	−	−	−	−

a dipolar-driven destabilization of the collinear ferromagnetic state. The DM interaction is the only driving force toward noncollinearity. In the following, the validity of Eq. (3) will be discussed in detail. In particular, it will be shown that the discussed approximation is appropriate for the micromagnetic description of closed Fe DL films on W(110). In a second step, it is shown that in Fe DL stripes of finite width, ε_d^* can no longer be neglected and must be taken into account in order to describe the experimentally observed stripe-width dependence of the spin spiral profile.

II. CLOSED FE DOUBLE-LAYER FILMS

In the studies summarized in Table I, the experimentally observed spin spiral state in the Fe DL on W(110) was investigated using micromagnetic calculations and Monte Carlo simulations. In Ref. 1, the spiral state is induced by the definition of appropriate boundary conditions. In Ref. 2, the observed magnetic structure is discussed in terms of classical domain theory where magnetic domains are formed due to the reduction of dipolar energy. References 3 and 4 consider the DM interaction as the dominating driving force toward noncollinearity. In all studies, the micromagnetic parameters A, K, and D were determined as fit parameters of the underlying micromagnetic models.

According to Table I, none of the suggested models allows for the explanation of all experimental observations. Therefore, it must be taken into account that all reported models can only be considered as effective models with effective model parameters A, K, and D. *A priori*, it is not clear whether these effective model parameters can be related to physically meaningful quantities such as exchange stiffness, magnetic anisotropy, and the DM vector, as was done in the studies summarized in Table I.

In the following, the previously suggested models will be compared and a critical discussion of the underlying assumptions will be given. For the extended Fe DL on W(110), it will be shown that, using the model described by Eq. (3), a consistent explanation of all experimental observations of the magnetic properties can be achieved. The description goes beyond all previous approaches and results into a unique set of micomagnetic parameters, which can be related to the physical quantities exchange stiffness, magnetic anisotropy, and the DM vector.

A. Exchange stiffness and effective anisotropy

Initially, the discussion is restricted to the micromagnetic models and the fitting procedures applied in Refs. 1 and 2. A major focus is put on the conflicting predictions and values of the micromagnetic parameters A and K_{eff}, as determined in these studies.

Starting from Eq. (1) and Refs. 1 and 2, we suggest that the inconsistencies between the models originate from two issues: (i) In both models, the DM interaction was omitted ($D = 0$). (ii) In Ref. 1, the micromagnetic parameters were determined by data fits with respect to the spiral shape, while in Ref. 2 they were obtained by fits to the spiral period.

1. Data fits with respect to the spiral period

In general, the period of magnetic domain patterns and spin spirals depends on the demagnetizing energy density (in particular ε_d^*) on the one hand and the domain-wall energy on the other hand. Starting from Eq. (3), the domain-wall energy can be calculated using variational techniques:[18]

$$E = \sqrt{A K_{\mathrm{eff}}} - \pi D. \tag{4}$$

As a direct consequence of this relationship, the spiral period increases with increasing values of A and K_{eff} and decreases with increasing values of D. Thus, the spiral period can be reproduced on the basis of infinitely many micromagnetic parameter sets (A, K_{eff}, D). In Ref. 2, one of these parameter sets ($D = 0$) was chosen arbitrarily by omitting the DM interaction. However, according to recent experimental results,[4,19,20] the assumption of a vanishing D is problematic in the context of ultrathin magnetic films.

2. Data fits with respect to the spiral shape

Like the domain-wall energy [Eq. (4)], the domain-wall profile, and thus even the profile of a complete spin spiral, can be calculated starting from Eq. (3) using variational techniques and appropriate boundary conditions. For a characteristic spiral sequence representing a full rotation of the magnetic moments by 360°, the field dependence of the spiral profile is described by[21]

$$\phi_{360}(x) = \sum_{+,-} \arcsin\left[\tanh\left(\frac{x \pm c}{w/2}\right)\right], \tag{5}$$

where

$$c := \frac{w}{2} \arcsin\left(\sqrt{\frac{2K_{\mathrm{eff}}}{M_S \mu_0 H}}\right) \tag{6}$$

and

$$w := 2\sqrt{\frac{A}{K_{\mathrm{eff}} + \frac{M_S}{2}\mu_0 H}}. \tag{7}$$

Here, M_S is the saturation magnetization, $\mu_0 H$ indicates the applied magnetic field, w is the width of a classical domain wall, and $2c$ is the field-dependent distance between two 180° walls being compressed by the external magnetic

field. Note that in contrast to the spiral period, the spiral profile is independent of D. Instead, it is fully characterized by the parameters A, K_{eff}, M_{S}, and $\mu_0 H$. Consequently, assuming a reasonable value of M_{S}, the parameters A and K_{eff} can be determined independently by fitting Eq. (5) to a field-dependent series of measured spiral profiles, as was done in Ref. 1. Since the spiral profile is independent of D, the fitting procedure remains applicable even in the presence of a significantly strong DM interaction. Thus, although the DM interaction was not considered in Ref. 1, the conclusions drawn remain valid even in the more general case of nonvanishing D. Consequently, the following analysis will be based on the parameter values reported in Ref. 1:

$$A = 1.8 \times 10^{-11}\ \mathrm{J/m}\,, \quad K_{\mathrm{eff}} = 1.25 \times 10^{6}\ \mathrm{J/m^3}. \tag{8}$$

B. Dzyaloshinskii-Moriya vector

Using the micromagnetic parameters of Eq. (8), the shape of the experimentally observed spiral profile and its magnetic field dependence for $B \geqslant 50$ mT can be reproduced using a micromagnetic model that does not consider the DM interaction.[1] However, in zero field, such a model fails and predicts a collinear magnetic ground state. In Ref. 1, this problem was overcome by inducing the spiral state on the basis of appropriate boundary conditions. In the following, it will be discussed that the boundary conditions can be dropped in the presence of a sufficiently strong DM interaction. In particular, in such a model, the direction of the DM vector can be determined by reproducing the experimentally observed propagation direction of the spin spiral, and thus the direction of the domain walls.[3,4] The magnitude of D is determined by reproducing the measured zero-field spiral period in addition to the previously discussed spiral shape and its magnetic field dependence.

1. Homogeneous spiral profiles

In analogy to the theoretical analysis in recent publications,[4,19,20] the discussion is first restricted to homogeneous, i.e., to continuously rotating, magnetization profiles:

$$\phi_\lambda(x) = \pm\frac{2\pi}{\lambda}x. \tag{9}$$

Here, the sign of $\phi(x)$ determines the rotational sense of the spin spiral, i.e., $(-)$ accounts for right-rotating and $(+)$ for left-rotating spirals, respectively. Using Eq. (9), Eq. (3) can be rewritten as

$$\varepsilon[\phi_\lambda] = 4\pi^2 A\lambda^{-2} - 2\pi D\lambda^{-1} + \frac{K_{\mathrm{eff}}}{2}. \tag{10}$$

Figure 1 shows all contributions to the energy density dispersion, as calculated for the Fe DL on W(110) on the basis of the parameter set of Eq. (8). Here, the energy density dispersions of right-rotating (left-rotating) spin spiral profiles are displayed in the right (left) half-plane of the graph. For the energy density contribution of magnetic exchange, one observes a parabolic behavior (solid black curve). The energy density dispersion of the effective anisotropy is independent of the spiral period (dashed green line) except for a discontinuous jump at $\lambda^{-1} = 0$ (green dot). This discontinuity is an artifact

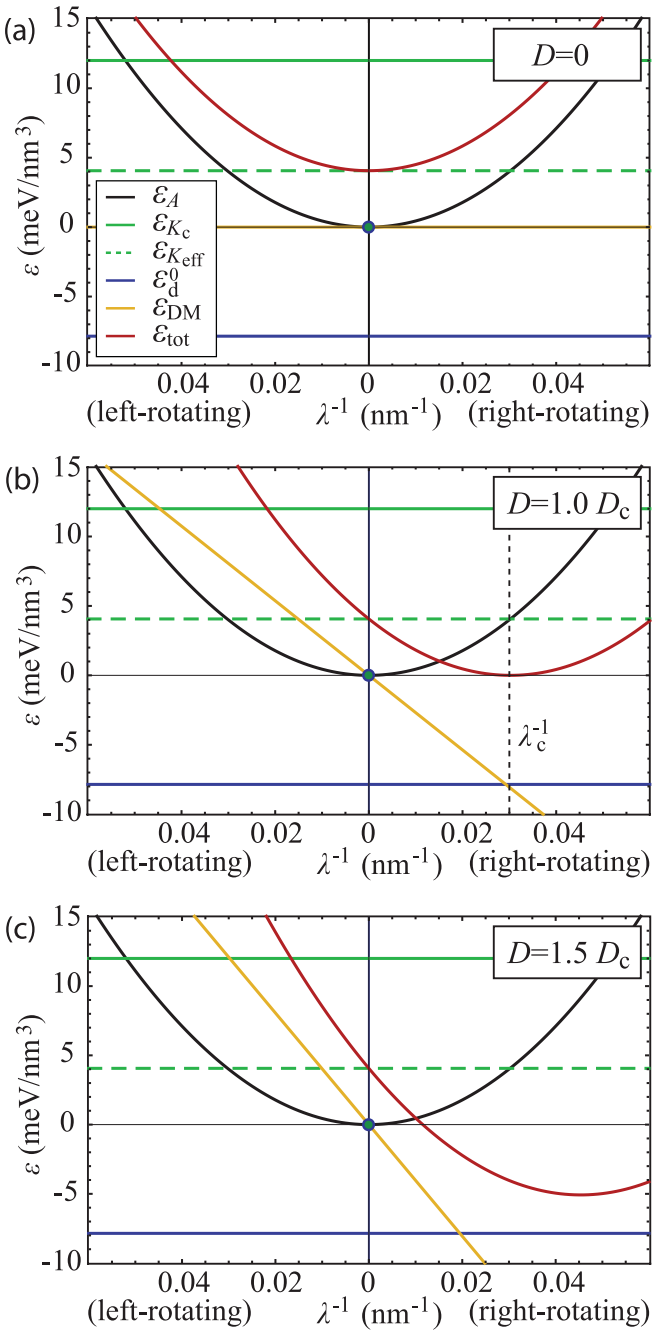

FIG. 1. (Color) Energy density dispersions, as calculated for the special case of homogeneous, i.e., sinusoidal, spiral profiles and various values of the Dzyaloshinskii parameter D. The solid green dot at the origin indicates the total energy density of the collinear single-domain state. Energy density dispersions of right-rotating (left-rotating) spin spiral profiles are displayed in the right (left) half plane of the graph. λ_c: maximum spiral period in the spiral regime.

of the *ad hoc* restriction to homogeneous spiral profiles that implies a finite spiral period λ and does not allow for a continuous transition between the spiral regime and the collinear ferromagnetic state. The energy density dispersion of the effective anisotropy can be separated into the two contributions of the crystalline (solid green line) and shape anisotropy (solid blue line). Finally, the DM interaction results in a linear dispersion relation with the slope being given by the

Dzyaloshinskii parameter D (yellow line). The figure displays three scenarios that correspond to three different values of D. In each case, the energy density of the collinear single domain state is given by the dot at the origin of the coordinate system.

For $D = 0$, the total energy density is described by a parabola with its minimum at $(0|\frac{K_{\text{eff}}}{2})$. For finite D, the parabola undergoes an additional linear displacement with the minimum of the parabola being shifted to

$$\left(-\frac{D}{4\pi A}\,\middle|\,-\frac{D^2}{4A}+\frac{K_{\text{eff}}}{2}\right). \tag{11}$$

The spin spiral state becomes favorable with respect to the ferromagnetic single-domain state if the minimum of the parabola is shifted to energy densities below the one of the ferromagnetic configuration, i.e., if the Dzyaloshinskii parameter D is larger than a certain critical value D_c, which can be determined on the basis of Eq. (11) (Ref. 19):

$$D > D_c = \sqrt{2}\sqrt{AK_{\text{eff}}}. \tag{12}$$

At $D = D_c$, the magnetic ground state undergoes a phase transition between the collinear state (dot in Fig. 1) and the spin spiral regime. The transition is accompanied by a discontinuous jump of the spiral period, as visualized in Fig. 1(b). The corresponding critical spiral period λ_c can be determined from the minimum of the energy dispersion Eq. (11):

$$\lambda_c = \frac{4\pi}{\sqrt{2}}\sqrt{\frac{A}{K_{\text{eff}}}} = \frac{2\pi}{\sqrt{2}}w_0. \tag{13}$$

This behavior implies that large spiral periods can only be reproduced by simultaneously increasing the value of λ_c. However, according to Eq. (13), λ_c is directly related to the domain-wall width w_0. Consequently, within the framework of a homogeneous spin spiral model, large spiral periods and narrow domain-wall profiles can not be reproduced simultaneously, i.e., on the basis of one single and unique set of micromagnetic parameters. In particular, the model fails in the description of the spin spiral in Fe DL on W(110) where the spiral period ($\lambda = 45$ nm) is significantly larger than the domain-wall width ($w_0 = 7$ nm).

Nevertheless, the homogeneous spiral model with its implicit coupling of the spiral period and the domain-wall width was applied in Ref. 4 also to the Fe DL on W(110). The micromagnetic parameters were obtained by reproducing the energy density dispersions calculated by density functional theory (DFT). Since the DFT calculations were also based on the assumption of homogeneous spiral profiles, the fit was almost perfect. However, the assumption of homogeneous, i.e., sinusoidal, spiral profiles becomes problematic when the reported exchange stiffness, magnetic anisotropy, and DM vector are compared to the experimental observations. In particular, the domain-wall width resulting from these parameters corresponds to about twice the experimentally observed value, i.e., roughly 1/4 of the spiral period, not unexpected for an assumed sinusoidal spiral profile.

2. *Inhomogeneous spin spiral profiles*

In order to overcome the discussed deficiencies, the following considerations refer to the general case of inhomogeneous spin spiral profiles. Within such an extended model approach, the domain-wall width and the spiral period are independent quantities, in contrast to the homogeneous spiral model discussed before. In particular, this allows for a consistent description of the spin spiral in the Fe DL on W(110).

For the generalized scenario of inhomogeneous spin spiral profiles, the analysis of the various contributions to the energy density dispersion Eq. (1) can be performed in formal analogy to the homogeneous case. In general the spiral profile can only be determined numerically. However, applying the same approximation as in the previous section, i.e., the concept of incorporating the demagnetizing energy into an effective anisotropy parameter according to Eq. (3), the exact solution of the spiral profile can be determined in an analytically closed form as derived in Ref. 22:

$$\begin{aligned}\phi(x) &= \pm\text{am}\left(\frac{1}{\delta\sqrt{\frac{A}{K_{\text{eff}}}}}x,\delta\right),\\ \lambda &= 4\delta\sqrt{\frac{A}{K_{\text{eff}}}}\text{F}\left(\frac{\pi}{2},\delta\right),\\ D &= \frac{4}{\pi\delta}\sqrt{AK_{\text{eff}}}\text{E}\left(\frac{\pi}{2},\delta\right).\end{aligned} \tag{14}$$

Here, am is the Jacobi amplitude function. It is defined as the inverse function of the complete elliptic integral of the first kind. The parameter $\delta \in [0,1]$ indicates the degree of inhomogeneity of the spiral profile. It is related to the spiral period λ and the Dzyaloshinskii parameter D via F and E, i.e., the incomplete elliptic integrals of the first and second kinds.[23] In the homogeneous limit ($\delta \to 0$, $D \gg \frac{4}{\pi}\sqrt{AK_{\text{eff}}}$), the Jacobi amplitude becomes a linear function of x, thus, $\phi(x)$ reduces to Eq. (9). With increasing δ, i.e., decreasing D, the Jacobi amplitude function deviates from this linear behavior. Consequently, the angle between two neighboring magnetic moments along the spin spiral is no longer independent of the spatial position x. The spin spiral becomes inhomogeneous.[24]

In contrast to the homogeneous case, $\phi(x)$ can no longer be written as a direct function of λ since the second expression in Eq. (14) can not be solved for δ. However, for a given value of δ, both λ and $\phi(x)$ can be determined. Consequently, the spiral profile and the energy density dispersions can be calculated as a parameter curve of δ. Figure 2 shows the calculated energy density dispersions in analogy to the homogeneous case visualized in Fig. 1. Again, the total energy density ε_{tot} (red curve) is given for three different values of the Dzyaloshinskii parameter D. For all three scenarios, the energy density of the collinear single-domain state is given by the dot at the origin of the coordinate system. In contrast to the homogeneous case, the total energy density dispersion is now pinned at the origin, i.e., it is no longer shifted due to crystalline and shape anisotropy. While the total energy density dispersion $\varepsilon_{\text{tot}}(\lambda^{-1})$ is symmetric for $D = 0$ [Fig. 2(a)], it is deformed toward an asymmetric shape for $D \neq 0$ [Figs. 2(b) and 2(c)]. As in the homogeneous case, the system undergoes a phase transition between the collinear state and the spin spiral regime if the Dzyaloshinskii parameter D becomes equal to a critical value D_c. In contrast to the homogeneous case, however, this critical

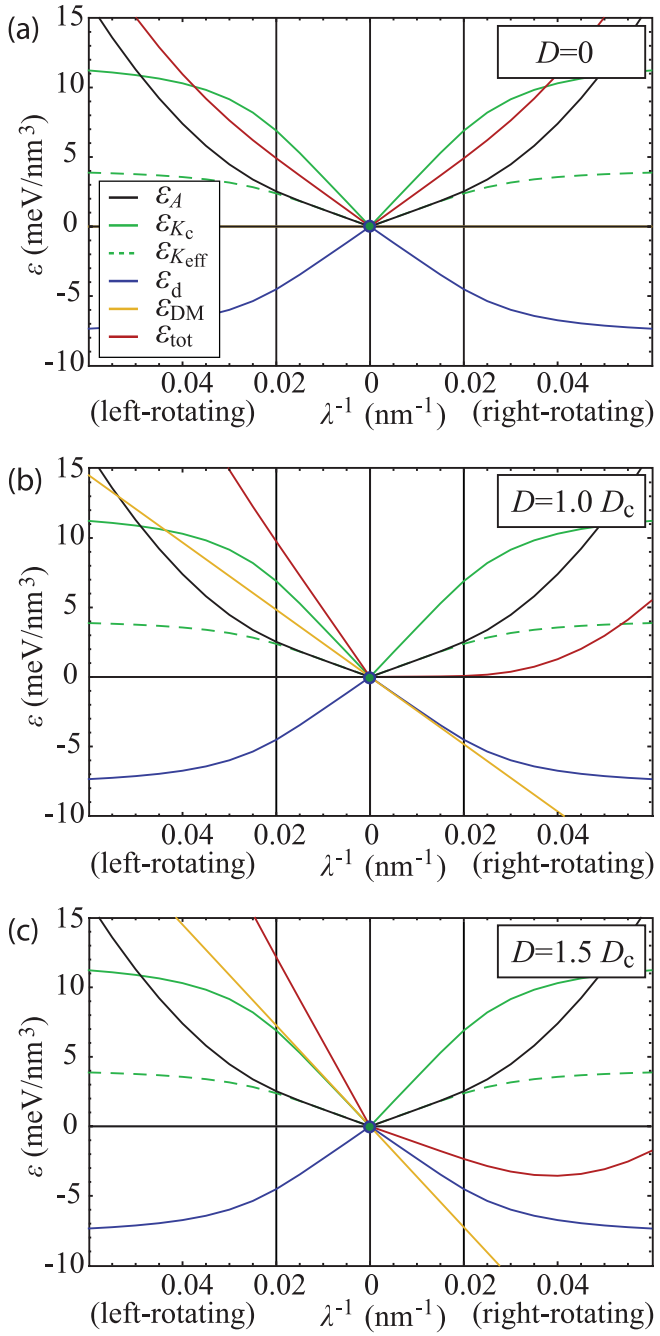

FIG. 2. (Color) Energy density dispersions as calculated for the case of inhomogeneous spiral profiles according to Eq. (14) and various values of the Dzyaloshinskii parameter D. The total energy density of the collinear single-domain state is visualized by the dot at the origin. Energy density dispersions of right-rotating (left-rotating) spin spiral profiles are displayed in the right (left) half plane of the graph (Ref. 25).

value is now given by[22,26]

$$D_c = \frac{4}{\pi}\sqrt{AK_{\text{eff}}}. \tag{15}$$

Again, right-rotating spin spirals are favored with respect to left-rotating ones due to the asymmetric character of the DM interaction [$\pm$ sign in Eq. (14)]. However, in contrast to the homogeneous scenario discussed before, the phase transition between the collinear and the spin spiral regimes is continuous. As a consequence, at $D = D_c$, the critical spiral period λ_c is no longer given by Eq. (13). Instead, one obtains

$$\lambda_c = \infty. \tag{16}$$

Thus, independent of the values of A and K_{eff}, the measured spiral period can be reproduced by increasing D to an appropriate value above D_c. Consequently, the inhomogeneous model allows us to simultaneously reproduce the magnetic field dependence and the spiral period. As discussed before, the magnetic field dependence of the spin spiral in the Fe DL on W(110) results in the parameter set given in Eq. (8).[1] The spiral period of 45 nm is reproduced for

$$D = 1.05D_c = 6.4 \times 10^{-3}\ \text{J/m}^2. \tag{17}$$

This value is by a factor of 2.26 larger than the value determined by DFT calculations with a subsequent fitting procedure on the basis of homogeneous spin spiral profiles.[4] According to the previous discussion of the homogeneous spiral model, this deviation is due to the fact that the parameters determined in Ref. 4 must be considered as the parameters of an effective micromagnetic model that describes the underlying DFT calculations, which rely on the assumption of homogeneous spiral profiles, i.e., on the unrealistic coupling of the parameters A, K_{eff}, and D.

In summary, it was shown that the spin spiral ground state in the Fe DL on W(110) can be described within the framework of a micromagnetic model that considers four different magnetic energy contributions (magnetic exchange, crystalline anisotropy, shape anisotropy, and the DM interaction) and allows for inhomogeneous spin spiral profiles. In particular, the model explains the observed spiral period, the unique rotational sense, the measured domain-wall width, the propagation direction, the direction of the domain walls, and the magnetic field dependence of the spiral profile in a consistent way. By comparison to Table I, it becomes clear that this is a first major step toward a comprehensive description of magnetism in the Fe DL on W(110). According to Eq. (17), the observed spin spiral state is induced because the DM interaction is strong enough to dominate the other interactions. However, this is only possible because of the dipolar interaction that reduces the crystalline to an effective anisotropy, which implicitly includes the contribution of ε_d^0. Without this dipolar energy contribution, the DM interaction would be too weak to destabilize the collinear state. Thus, it is the joint effect of both interactions that induces the spiral state.[27]

III. FE DOUBLE-LAYER STRIPES OF FINITE WIDTH

In the preceding section, the focus was put on the analysis of the spin spiral in the *extended* Fe DL on W(110). It was shown that the spin spiral is induced by the interplay of magnetic exchange, anisotropy, and the DM interaction. The demagnetizing energy was considered in terms of an effective anisotropy parameter. In particular, it was shown that the observed spiral period, the unique rotational sense, the domain-wall width, the domain-wall orientation, and the magnetic field dependence (first five rows in Table I) can be reproduced consistently on the basis of an extended

micromagnetic model and a unique set of micromagnetic parameters. In the following, the micromagnetic model is extended to Fe DL stripes *of finite width* on W(110), as investigated in previous SP-STM experiments.[8,10,28] The main focus is put on the investigation of the observed vanishing of the spin spiral ground state in narrow stripes, the stripe-width-dependent vanishing of the spin contrast at elevated temperatures, and the stripe-width dependence of the spiral period (last three rows in Table I).

A. Extended micromagnetic model

Up to now, all micromagnetic calculations were restricted to the case of extended Fe DL films on W(110), i.e., the magnetization was assumed to be constant along the direction perpendicular to the propagation direction of the spin spiral. Consequently, inhomogeneities of the demagnetizing field at the edges of the Fe DL areas could be neglected. For an appropriate description of Fe DL stripes of finite width, these simplifications must be dropped in the following. Thus, it is assumed that inside the Fe DL stripes, the magnetization remains constant along the direction perpendicular to the propagation direction, while it is assumed to be zero in the gaps between the stripes [cf. Fig. 3(a)]. Compared to the experimentally investigated samples, this assumption constitutes a simplification since in real systems the DL stripes are separated by in-plane magnetized monolayer (ML) areas [cf. Fig. 3(b)]. According to Ref. 29, the ML is ferromagnetic below its Curie temperature $T_c = 225$ K with an in-plane-anisotropy along $[1\bar{1}0]$. Nevertheless, neglecting the magnetic structure of the ML seems to be well justified since, due to the in-plane anisotropy, the Fe ML only has a weak stray field that is oriented perpendicular to the magnetization in the DL and therefore should not affect the magnetization of the DL stripes significantly.

For an Fe DL stripe array like the one shown in Fig. 3(a), the topography can be described by a function varying only along the y direction perpendicular to the stripes:

$$\tau(y) = \begin{cases} 1: & n\lambda_y \geqslant y \geqslant n\lambda_y + b, \\ 0: & n\lambda_y + b > y > (n+1)\lambda_y. \end{cases} \tag{18}$$

Here, a value of 1 indicates areas that are covered by the Fe film, a value of 0 refers to the nonmagnetic areas of the bare substrate, and n is defined to be an integer ($n \in \mathbb{N}$). In agreement with the measurements presented in Refs. 8,10, and 28 and the discussion in Sec. II, in the following, the propagation direction of the spin spiral is assumed to be oriented along the x axis. Thus, the two-dimensional functions $\sigma(x,y)$ and $\gamma(x,y)$ can be defined as

$$\begin{aligned} \sigma(x,y) &= \sin[\phi(x)]\,\tau(y) = \frac{M_z}{M_S}(x,y), \\ \gamma(x,y) &= \cos[\phi(x)]\,\tau(y) = \frac{M_x}{M_S}(x,y). \end{aligned} \tag{19}$$

Based on these functions, the total energy density can be calculated starting from Eq. (1) with ε_d now being defined as

$$\varepsilon_d = \frac{1}{p}\left\{\varepsilon_d^{\sigma}[\sigma(x,y)] + \varepsilon_d^{\gamma}[\gamma(x,y)]\right\}. \tag{20}$$

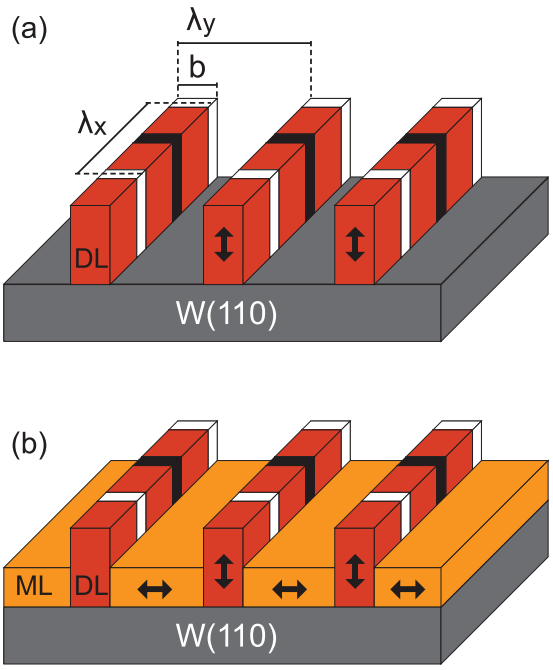

FIG. 3. (Color) (a) Magnetic configuration, as used for the calculations in this paper. The ML areas are not considered since the spiral profile in the DL is essentially unaffected by the ML due to the perpendicular orientation of the magnetic easy axis. (b) Magnetic configuration of the Fe DL stripes on W(110) and the intermediate Fe ML. In the ML areas, the magnetic easy axis points perpendicular to the propagation direction of the spin spiral in the DL.

Here, p denotes the surface fraction covered by magnetic material such that the energy density ε_d refers to the energy per magnetic volume. The two summands ε_d^{σ} and ε_d^{γ} are calculated according to[18,30,31]

$$\varepsilon_d^{\sigma}[\sigma(x,y)] = \frac{\mu_0}{2}M_S^2 d\left\{c_{00}^2 + {\sum_{rs}}'\left[|c_{rs}|^2\frac{1-e^{-2\pi g_{rs}}}{2\pi g_{rs}}\right]\right\}. \tag{21}$$

The summation $\sum'_{rs}$ is defined for integers r and s from $-\infty$ to $+\infty$, except for $r = s = 0$. The coefficients c_{rs} are defined as

$$\begin{aligned} c_{rs} &:= \int_0^{\lambda_y}\int_0^{\lambda_x}\left[\frac{\sigma(x,y)}{\lambda_x\lambda_y}e^{-2\pi i\left(r\frac{x}{\lambda_x}+s\frac{y}{\lambda_y}\right)}\right]dx\,dy, \\ g_{rs} &:= d\sqrt{\left(\frac{r}{\lambda_x}\right)^2 + \left(\frac{s}{\lambda_y}\right)^2}. \end{aligned} \tag{22}$$

In an analogous way, ε_d^{γ} calculates as

$$\begin{aligned} \varepsilon_d^{\gamma}[\gamma(x,y)] = \frac{\mu_0}{2}M_S^2 d\Bigg\{a_{00}^2 \quad &+ {\sum_{rs}}'\Bigg[|a_{rs}|^2\frac{\lambda_x^2}{\lambda_x^2+\lambda_y^2} \\ &\times\left(1-\frac{1-e^{-2\pi\kappa_{rs}}}{2\pi\kappa_{rs}}\right)\Bigg]\Bigg\}, \end{aligned} \tag{23}$$

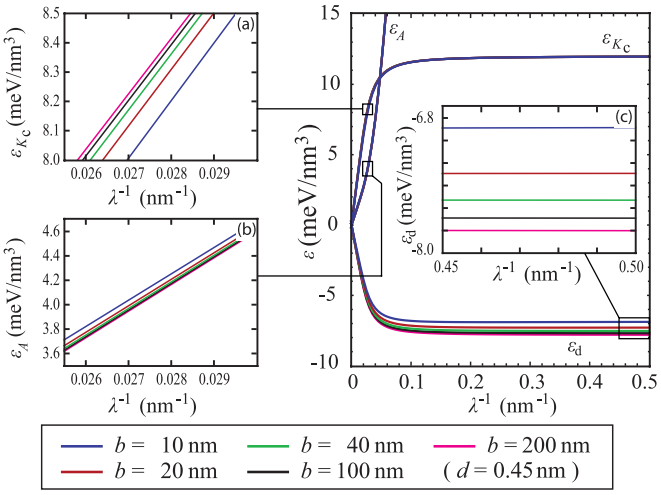

FIG. 4. (Color) Magnetic exchange ε_A, crystalline anisotropy ε_{K_c}, and demagnetizing energy density ε_d as a function of the inverse spiral period λ^{-1}. The curves were calculated for an array of Fe DL stripes with an interstripe distance $\lambda_y = 200$ nm. All dispersion relations show a clear stripe-width dependence, as shown in the insets.

with

$$a_{rs} := \int_0^{\lambda_y}\int_0^{\lambda_x}\left[\frac{\gamma(x,y)}{\lambda_x\lambda_y}e^{-2\pi i\left(r\frac{x}{\lambda_x}+s\frac{y}{\lambda_y}\right)}\right]dx\,dy,$$
$$\kappa_{rs} := d\sqrt{\left(\frac{r}{\lambda_x}\right)^2+\left(\frac{s}{\lambda_y}\right)^2}. \quad (24)$$

B. Calculated energy density dispersions

Starting from the micromagnetic model [Eqs. (1) and (18)–(24)], the spiral profile and the energy density dispersions $\varepsilon_A(\lambda^{-1})$, $\varepsilon_{K_c}(\lambda^{-1})$, $\varepsilon_{DM}(\lambda^{-1})$, and $\varepsilon_d(\lambda^{-1})$ can be calculated in formal analogy to the one-dimensional closed-film scenario of Sec. II. Figure 4 shows the energy density dispersions as calculated for stripe widths between $b = 10$ and 100 nm. The interstripe distance of $\lambda_y = 200$ nm was chosen such that, within the precision of the graphical representation, the calculated energy density dispersions do not change upon further increase of λ_y. Thus, it is guaranteed that the results refer to individual stripes that are not affected by dipolar coupling to neighboring stripes. The limit case $b = 200$ nm (magenta curve) was added as a reference. It refers to a stripe array with neighboring stripes being merged. It is geometrically equivalent to the closed-film geometry discussed in Sec. II [Eqs. (8) and (17)]. The curve was checked for consistency with the corresponding curve in Fig. 2, as calculated using Eq. (3). The results coincide within the precision of the graphical representation. This clearly indicates that, for the special case of closed Fe DL films on W(110), Eqs. (1) and (3) are essentially equivalent. In particular, this gives an *ex post* justification of the application of Eq. (3) in Sec. II and allows for the generalized use of the determined micromagnetic parameters [Eq. (8)] even in the context of the more sophisticated model equation (1).

The calculation of all curves in Fig. 4 is based on the idea that all micromagnetic parameters are independent of the stripe width. Taking into account that they describe local properties, and thus essentially depend on the local lattice structure in the Fe DL, a variation of A, K_c, D, and M_S can only be expected in very close proximity to the stripe edges. Thus, it seems to be a reasonable assumption that the stripe-width dependence of the parameters can be neglected for $b > 10$ nm (more than 40 atomic distances), as discussed in the present context. Despite this assumption, $\varepsilon_A(\lambda^{-1})$, $\varepsilon_{K_c}(\lambda^{-1})$, and especially $\varepsilon_d(\lambda^{-1})$ show an explicit stripe-width dependence (cf. insets in Fig. 4). The stripe-width dependence of $\varepsilon_A(\lambda^{-1})$, $\varepsilon_{K_c}(\lambda^{-1})$ only exists in the regime of inhomogeneous spiral profiles and fully disappears in the homogeneous limit ($\lambda^{-1} = \infty$). In contrast, the stripe-width dependence of $\varepsilon_d(\lambda^{-1})$ [Fig. 4(c)] prevails for homogeneous spiral profiles and decreases when approaching the inhomogeneous limit ($\lambda^{-1} = 0$). This inverse behavior can be attributed to two mechanisms:

(i) The total demagnetizing energy density ε_d decreases with increasing values of λ^{-1}. For closed films ($b = 200$ nm) and in the homogeneous limit, it converges to $-\frac{\mu_0}{2}M_S^2$, in agreement with the calculations of Sec. II. Note that, according to Fig. 4, the value to which the energy converges increases with decreasing stripe width, as shown in Fig. 4(c). This effect originates from the energy density contribution of ε_d^* that varies as a function of the stripe width due to the varying significance of the demagnetizing field inhomogeneities at the stripe edges.

(ii) As a second-order effect, the stripe-width dependence of the demagnetizing energy density results in a stripe-width dependence of the profile $\phi(x)$. The effect only plays a role in the regime of inhomogeneous spiral profiles and vanishes in the homogeneous limit, where the spiral profile is perfectly sinusoidal by definition. In narrow stripes, the variation of $\phi(x)$ reflects the reduced domain-wall width due to the reduced demagnetizing energy density (ε_d^0) and the increased value of K_{eff}. As a consequence of this reduced domain-wall width, the exchange energy density ε_A increases with decreasing stripe width [Fig. 4(a)], while the crystalline anisotropy energy density ε_{K_c} decreases [Fig. 4(b)]. In contrast, $\varepsilon_{DM}(\lambda^{-1})$ is independent of the shape of the spiral profile and only depends on the spiral period, as discussed in Sec. II. Consequently, it is not affected by the variation of $\phi(x)$ and remains unchanged with respect to Fig. 2.

C. Stripe-width dependence of the spin spiral ground state

Starting from the energy density dispersions of Fig. 4, it is straightforward to calculate the total energy density dispersion and investigate its stripe-width dependence. Figure 5 shows the result for various stripe widths. Again, the Dzyaloshinskii parameter [$D = 6.4 \times 10^{-3}$ J/m^2, in agreement with Eq. (17)] was chosen such that the position of the global energy density minimum reflects the experimentally observed spiral period $\lambda = 45$ nm in an infinitely extended closed Fe DL film ($b = 200$ nm, magenta curve). The result was checked for consistency with the result of the one-dimensional calculation in Sec. II. The curves coincide within the accuracy of the graphical representation.

1. *Stripe-width dependence of the spiral period*

With decreasing stripe width, the depth of the total energy density minimum gradually decreases and shifts toward

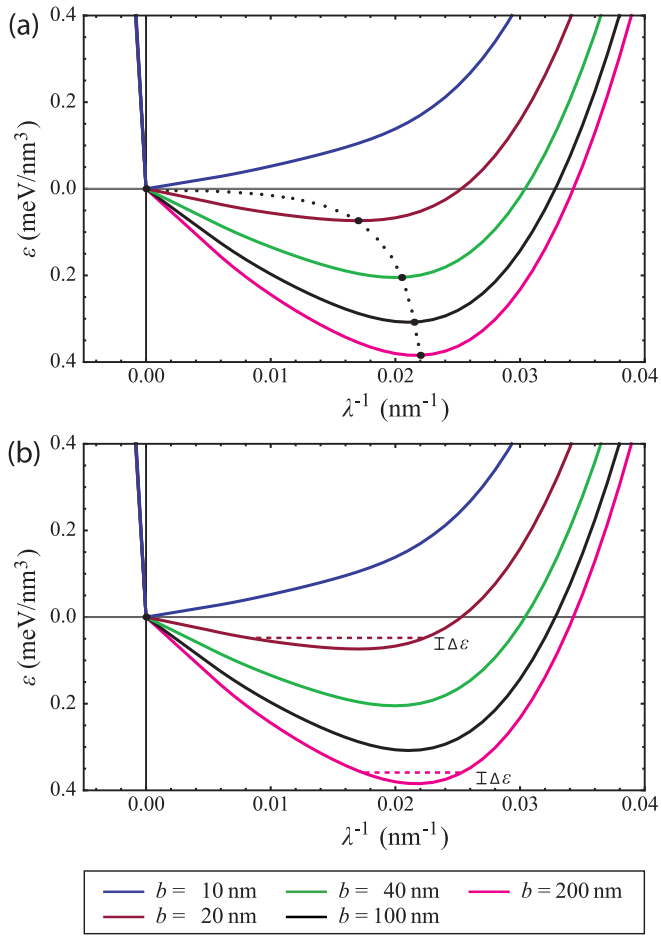

FIG. 5. (Color) Stripe-width dependence of the dispersion of the total energy density. The magenta curves represent the closed Fe DL film and coincide with the respective solution, as calculated in Sec. II. (a) With decreasing stripe width, the energy density minimum shifts to higher energy densities and larger spiral periods (black dotted curve). (b) At finite temperature, indicated by $\Delta\varepsilon$, the width of the energy density minimum depends on the stripe width, as indicated by the dashed horizontal lines.

smaller values of λ^{-1}, i.e., larger spiral periods [black dotted line in Fig. 5(a)]. For stripe widths between 200 and 20 nm, the spiral period varies between 45.5 and 58.8 nm, respectively. Below $b = 20$ nm, the spiral period increases dramatically and eventually reaches values in the micrometer regime. The calculated dependence of the energy density minimum on the geometrical stripe width is in very good agreement with experimental observations.[8,10] Thus, the model describes the hitherto unexplained vanishing of the spiral state for narrow stripe geometries.[10] In particular, the calculations are in good quantitative agreement with the experimental finding of a critical stripe width of about 15 nm. In addition to the vanishing of the spin spiral, the results of Fig. 5 predict a continuous transition from the spiral state to the ferromagnetic state. The calculated transition path (black dotted line) is in good quantitative agreement with previous measurements,[8] where the discussed variation of the spiral period was observed by SP-STM. However, in Ref. 8, the varying period of the spiral state was attributed to the Fe coverage on the W(110) substrate, i.e., to the ratio of stripe width and interstripe distance. In contrast to this interpretation, the energy density dispersions in Fig. 5 indicate that the variation can be explained without considering the influence of neighboring stripes. Thus, the measured variation of the spiral period is suggested to be a property of freestanding stripes, which can solely be explained by the variation of the stripe width in the experiments, i.e., the variation of ε_d due to the varying significance of the demagnetizing field inhomogeneities at the stripe edges.

2. *Stripe-width dependence of the ground-state energy density*

In addition to the stripe-width dependence of the ground-state spiral period, the calculations visualized in Fig. 5 also predict a stripe-width dependence of the thermal stability of the spin spiral. The depth of the global energy density minimum decreases with decreasing stripe width. Consequently, the energy difference between the spiral state and the ferromagnetic state decreases as well and can eventually be overcome by thermal excitations at finite temperatures. According to Fig. 5, the spiral state in narrow stripes (red) can be excited at lower temperature as compared to wider stripes (green, black) and closed films (magenta). In addition, the energy minimum broadens with decreasing stripe width [dashed horizontal lines in Fig. 5(b)]. Thus, even if the spiral state can not be excited to the ferromagnetic configuration, the range of accessible spiral periods at finite temperature increases with decreasing stripe width. Consequently, the calculations are compatible with a temperature-driven excitation of the magnetic state that results in the vanishing spin contrast observed in SP-STM experiments performed at elevated temperature. In particular, the calculations predict a critical temperature that increases with increasing stripe width, in good qualitative agreement with previous SP-STM measurements.[8]

IV. SUMMARY

In order to describe the properties of the spin spiral in the Fe DL on W(110), various micromagnetic models were proposed during the past years.[1–4] However, these approaches turned out to be contradictory to at least some of the experimental observations (cf. Table I). In this paper, the discussed contradictions could be resolved by the development of an extended micromagnetic model. In particular, the previously suggested models were simultaneously extended along two directions: (i) In addition to magnetic exchange, crystalline anisotropy, and the homogeneous contribution to the demagnetizing energy, the model accounts for the DM interaction and the energy contribution of inhomogeneities in the demagnetizing field. (ii) The restriction to homogeneous sinusoidal spiral profiles was dropped and the considerations were extended to arbitrary, i.e., inhomogeneous, spiral profiles. Based on this comprehensive micromagnetic model, the micromagnetic parameters A, K_c, and D were determined as fitting parameters to the measured spin spiral profile. The value of M_S was estimated from the respective value in bulk Fe, in agreement with Ref. 1. In contrast to the models of Table I, the parameter set is unique and the calculations are consistent with all experimental observations known to date.

In particular, the discussed calculations indicate a functional relationship between the spiral period and the stripe geometry that originates from the reduced demagnetizing energy density in narrow stripes. Thus, according to our calculations, it is in principle feasible to tailor the spiral period in Fe DL stripes on W(110) by adjusting the stripe width in an appropriate way. This may be of particular interest for future experiments and even technological applications.

ACKNOWLEDGMENTS

Financial support from the Deutsche Forschungsgemeinschaft (SFB 668-A8), the ERC Advanced Grant FURORE, and the Hamburg Cluster of Excellence NANOSPINTRONICS is gratefully acknowledged. N.M. acknowledges funding by Proyecto CONSOLIDER-INGENIO EN NANOCIENCIA MOLECULAR Ref. No. CSD2007-00010, by the Comunidad de Madrid through Project No. S2009/MAT-1726.

*smeckler@physnet.uni-hamburg.de

[1] A. Kubetzka, O. Pietzsch, M. Bode, and R. Wiesendanger, Phys. Rev. B **67**, 020401(R) (2003).

[2] E. Y. Vedmedenko, A. Kubetzka, K. von Bergmann, O. Pietzsch, M. Bode, J. Kirschner, H. P. Oepen, and R. Wiesendanger, Phys. Rev. Lett. **92**, 077207 (2004).

[3] S. Meckler, N. Mikuszeit, A. Preßler, E. Y. Vedmedenko, O. Pietzsch, and R. Wiesendanger, Phys. Rev. Lett. **103**, 157201 (2009).

[4] M. Heide, G. Bihlmayer, and S. Blügel, Phys. Rev. B **78**, 140403(R) (2008).

[5] A. Kubetzka, Ph.D. thesis, Universität Hamburg, 2002.

[6] M. Bode, K. von Bergmann, A. Kubetzka, O. Pietzsch, and R. Wiesendanger, J. Magn. Magn. Mater. **304**, 1 (2006).

[7] M. Bode, A. Kubetzka, S. Heinze, O. Pietzsch, R. Wiesendanger, M. Heide, X. Nie, G. Bihlmayer, and S. Blügel, J. Phys.: Condens. Matter **15**, 679 (2003).

[8] K. von Bergmann, M. Bode, and R. Wiesendanger, J. Magn. Magn. Mater. **305**, 279 (2006).

[9] J. Hauschild, H. J. Elmers, and U. Gradmann, Phys. Rev. B **57**, R677 (1998).

[10] O. Pietzsch, Ph.D. thesis, University of Hamburg, 2001.

[11] H. J. Elmers, J. Hauschild, and U. Gradmann, Phys. Rev. B **59**, 3688 (1999).

[12] H. J. Elmers, J. Hauschild, and U. Gradmann, J. Magn. Magn. Mater. **198**, 222 (1999).

[13] M. Heide, Ph.D. thesis, RWTH Aachen, Germany, 2006.

[14] I. E. Dzyaloshinskii, Zh. Eksp. Teor. Fiz. **32**, 1547 (1957) [Sov. Phys.–JETP **5**, 1259 (1957)].

[15] I. Dzyaloshinsky, J. Phys. Chem. Solids **4**, 241 (1958).

[16] T. Moriya, Phys. Rev. **120**, 91 (1960).

[17] T. Moriya, Phys. Rev. Lett. **4**, 228 (1960).

[18] A. Hubert and R. Schäfer, *Magnetic Domains* (Springer, Berlin, 1998).

[19] M. Bode, M. Heide, K. von Bergmann, P. Ferriani, S. Heinze, G. Bihlmayer, A. Kubetzka, O. Pietzsch, S. Blügel, and R. Wiesendanger, Nature (London) **447**, 190 (2007).

[20] P. Ferriani, K. von Bergmann, E. Y. Vedmedenko, S. Heinze, M. Bode, M. Heide, G. Bihlmayer, S. Blügel, and R. Wiesendanger, Phys. Rev. Lett. **101**, 027201 (2008).

[21] H.-B. Braun, Phys. Rev. B **50**, 16485 (1994).

[22] Y. A. Izyumov, Usp. Fiz. Nauk. **144**, 439 (1984) [Sov. Phys. Usp. **27**, 845 (1984)].

[23] M. Abramowitz and I. M. Stegun, *Handbook of Mathematical Functions* (Dover, New York, 1965).

[24] The Jacobi amplitude is not the exact solution to Eq. (1), which can only be determined numerically. However, the numerically calculated spiral profiles turn out to coincide with the spiral profile resulting from Eq. (14) within the precision of our graphical representation. Since the spiral profile is independent of the Dzyaloshinskii parameter D, as discussed in the previous section, the profile also coincides with the spiral profiles fitted to the experimental data in Ref. 1.

[25] Note that the energy density dispersions in Fig. 2 deviate from those presented in Fig. 4, Ref. 3. The origin of this deviation is twofold: (i) In contrast to Ref. 3, the calculations rely on the micromagnetic parameters of Eq. (8) in order to allow for the description of the measured magnetic field dependence. (ii) In Ref. 3, the effect of the demagnetizing energy on the formation of the spin spiral state was overestimated by a factor of 2 due to a computational error. This deficiency was corrected in the figure shown here.

[26] I. E. Dzyaloshinskii, Zh. Eksp. Teor. Fiz. **47**, 992 (1964) [Sov. Phys.–JETP **20**, 665 (1965)].

[27] S. Meckler, Ph.D. thesis, Universität Hamburg, 2010.

[28] M. Bode, A. Kubetzka, O. Pietzsch, and R. Wiesendanger, Appl. Phys. A **72**, 149 (2001).

[29] H. J. Elmers, J. Hauschild, H. Höche, U. Gradmann, H. Bethge, D. Heuer, and U. Köhler, Phys. Rev. Lett. **73**, 898 (1994).

[30] E. Y. Tsymbal, Appl. Phys. Lett. **77**, 2740 (2000).

[31] N. Mikuszeit, S. Meckler, R. Wiesendanger, and R. Miranda, Phys. Rev. B **84**, 054404 (2011).